Nanoscale

Cite this: *Nanoscale*, 2011, **3**, 3747

www.rsc.org/nanoscale

PAPER

The development of a silica nanoparticle-based label-free DNA biosensor†

Arnold J. Kell,*[a] Lilianne Pagé,[a] Sophie Tan,[a] Isabelle Charlebois,[b] Maurice Boissinot,[b] Mario LeClerc[c] and Benoit Simard[a]

Received 28th April 2011, Accepted 15th June 2011
DOI: 10.1039/c1nr10435g

A silica nanoparticle-based DNA biosensor capable of detecting *Bacillus anthracis* bacteria through the use of unlabelled ss-oligonucleotides has been developed. The biosensor makes use of the optical changes that accompany a nanoparticle-immobilized cationic conjugated polymer (polythiophene) interacting with single-stranded *vs.* hybridized oligonucleotides, where a fluorescence signal appears only when hybridized DNA is present (*i.e.* only when the ss-oligonucleotide interacting with the polymer has hybridized with its complement). In order to enhance the sensitivity of the biosensor, two different nanoparticle architectures were developed and used to elucidate how the presence of neighboring fluorophores on the nanoparticle surface affects Förster-resonant energy transfer (FRET) between the polythiophene/oligonucleotide complex (FRET donor) and the fluorophores (FRET acceptors). We demonstrate that the silica nanoparticle-based FRET platform lowers the limit of detection at least 10-fold in comparison to the polythiophene itself, and allows the detection of $\sim 2 \times 10^{-12}$ moles of ss-oligonucleotide in a 100 μL sample with a standard fluorimeter (*i.e.* has a limit of detection of ~2 nM ssDNA). Such nanoparticle-based biosensor platforms are beneficial because of the robustness and stability inherent to their covalent assembly and they provide a valuable new tool that may allow for the sensitive, label-free detection (the target DNA that produces the fluorescence signal is unlabelled) without the use of polymerase chain reaction.

Introduction

There is significant interest in the development of rapid, sensitive, and specific methods for the detection of infectious diseases and protein biomarkers. Recently a number of teams have developed conjugated polymers that make use of conformational changes in the polymer backbone upon interaction with specific analytes to transduce optical signals when targets are present.[1–3] Though such polymer-based detection assays can identify whole bacteria,[4–6] there is also significant interest in identifying biological targets based on a DNA "fingerprint". An innovative strategy developed by Leclerc *et al.* has demonstrated the ability to detect unlabelled target oligonucleotides.[7] This label-free mode of detection involves the use of a conjugated polymer capable of transducing a fluorescence signal following the hybridization of complementary oligonucleotides (oligomers). The actual mechanism involved in the biosensing is highlighted in Scheme 1, where a fluorescent and positively charged polythiophene will form a duplex structure upon mixing with a negatively charged, single-stranded-oligomer (ss-oligomer).[7] As the polythiophene wraps around the probe ss-oligomer to form the duplex structure, its backbone will become more rigid and planar leading to significant changes in both the optical and fluorescence properties of the polymer.[7] Specifically, the UV-visible absorption maximum of the polymer is red-shifted and because the absorption band of the polymer is shifted in this duplex structure, it is no longer fluorescent when excited at 420 nm. However, upon hybridization with a complementary (target) ss-oligomer, the polymer backbone returns to a twisted structure similar to that of the free polymer, the absorption maximum blue-shifts near its original absorption maximum, and the fluorescence signal "turns on" to signal that a hybridization event has occurred. Leclerc and coworkers have extended the utility of these polythiophene-based biosensors by labeling the probe ss-oligomer with an appropriate fluorophore (Cy3 or Alexa Fluor 546), where hybridization with the target results in an increase in the emission intensity of the fluorophore through a Förster resonance energy transfer (FRET) mechanism.[7] This requires only that the absorption of the fluorophore (FRET acceptor, Alexa Fluor 546, AF546) overlaps with the emission of the polythiophene (FRET donor). If this condition is satisfied, the presence of the target oligomers will lead to hybridization

[a]*Steacie Institute for Molecular Sciences, National Research Council, 100 Sussex Drive, Ottawa, Ontario, Canada K1A 0R6. E-mail: arnold.kell@nrc.ca*
[b]*Centre de recherche en infectiologie de l'Université Laval, Centre hospitalier universitaire de Québec, Pavillon CHUL, Sainte-Foy, Québec, G1V 4G2, Canada*
[c]*Canada Research Chair in Electroactive and Photoactive Polymers, Département de Chimie, Université Laval, Sainte-Foy, Québec, G0A 1V6, Canada*
† Electronic supplementary information (ESI) available. See DOI: 10.1039/c1nr10435g

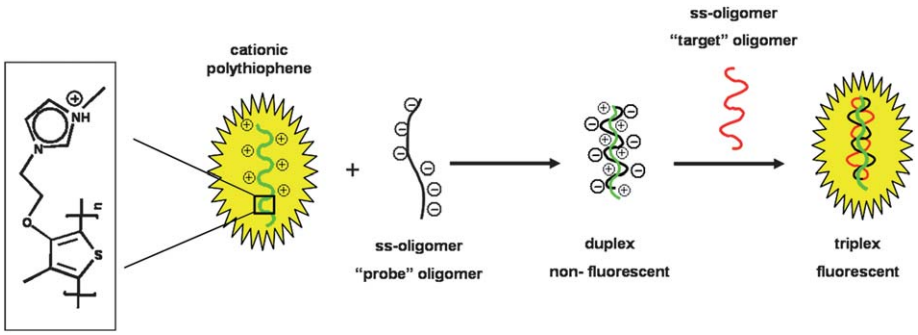

Scheme 1 Schematic description of the formation of polythiophene/single-stranded nucleic acid duplex and polythiophene/hybridized nucleic acid triplex forms.

between the probe oligomer and the target, resulting in a "turn on" of the emission of the polymer which will transfer energy to the FRET acceptor, increasing the emission intensity from the FRET acceptor (Scheme 2). This is beneficial because the quantum yield of AF546 is ~26 times greater than that of the polythiophene (0.79 *vs.* 0.03) so the resulting response to the hybridization event should be enhanced significantly (*i.e.* the polymer fluorescence can be transduced by the AF546 molecules).[7] The use of this FRET mechanism for biosensing is also useful because the emission of the AF546 moiety is markedly sharper in comparison to the broad emission of the polythiophene, so the ability to distinguish between the turn-on of fluorescence, particularly at low concentration, can be simplified greatly. The solution properties of these FRET-based biosensors are somewhat complicated, where it has been demonstrated that the duplex structures actually assemble into long rod shaped micelles with the fluorophores forming the core and the oligomer/polythiophene forming the corona (Scheme 3).[8] Because there is this high local concentration of fluorophore (FRET acceptor) at the core of the micelle, it has been proposed that if even a few of the duplex structures in the corona hybridize with a target ss-oligomer and become emissive (FRET donors), there are many FRET acceptors (AF546) in close proximity to the donor, so the intensity of the emission of the FRET acceptor is quite sensitive to the "turn on" of even a few polythiophene "transducers".[8] Though this micelle based system provides highly sensitive solution-phase detection, the fact that the system requires that the micelles stay intact does not make it robust with respect to changes in solvent conditions (salt, buffer and concentration) and makes it difficult to utilize in more general device-based applications where it would have to be immobilized on solid supports. As such, the development of similar but more robust, covalent assemblies of these polymer-based biosensors on nanoparticle scaffolds can potentially allow the biosensor to be employed in less controlled environments such as a deployable sensor.

Cationic polymer-based nucleic acid biosensing has previously been carried out on magnetic microparticles,[9] agarose beads[10] and silica nanoparticles.[11,12] The investigations utilizing magnetic nanoparticles[9] and agarose beads[10] were performed with the method highlighted in Scheme 1, where the duplex structure was immobilized on the surface of the beads and the resulting detection is based on the increase in luminescence intensity that accompanies the hybridization of the duplex with the target oligomer. Both of these platforms require customized equipment to analyse the biosensing that are not readily available to most researchers, though the sensitivity of both assays is quite good. In the case of the silica nanoparticle platform,[11] a FRET based approach was developed but the mechanism by which the sensor operates differs from that outlined in Scheme 2. Specifically the sensing protocol developed by Liu relies on fluorescein-labeled target oligomers (*i.e.* is not label-free) and utilizes a hybridization step prior to adding the conducting (transducing) polymer.[11] This biosensing scheme works quite well because FRET only occurs if the fluorophore-labeled target oligomer hybridizes with the nanoparticle-bound probe oligomer so there is very little

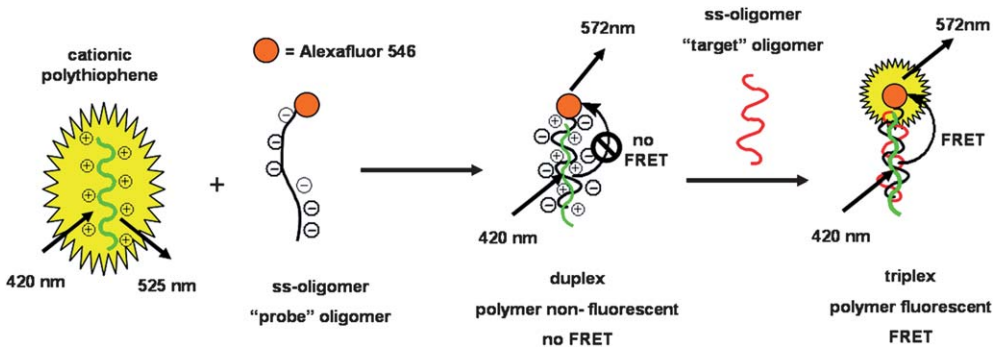

Scheme 2 Schematic description of the formation of polythiophene/AlexaFluor546-modified single-stranded nucleic acid duplex and polythiophene/hybridized nucleic acid triplex forms.

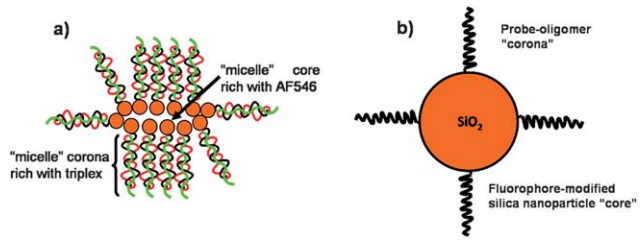

Scheme 3 Schematic description of the (a) rod-like micelle model of the ss-oligomer/polythiophene aggregates and (b) the nanoparticle scaffolds developed to mimic the aggregates.

background emission from the direct excitation of the fluorophore (*i.e.* the acceptor is only present if hybridization occurs). In another example, fluorophore-doped silver@silica core–shell nanoparticles can provide polymer based FRET detection of oligomers, though the detection requires significant nanoparticle aggregation and specialized imaging flow-cytometry equipment to signal the hybridization events.[12] We had interest in developing a sensor that could better mimic the micelle-based biosensor developed by Leclerc *et al.*,[7,8] where unlabelled oligomer targets can be detected. Here, we highlight the development of two different nanoparticle architectures where AF546-based FRET acceptors are immobilized on the surface of a silica nanoparticle and are surrounded by ss-oligomer/polythiophene ("duplex") structures (Fig. 1), mimicking the micelle-like structures reported by Leclerc. Within these architectures, the AF546

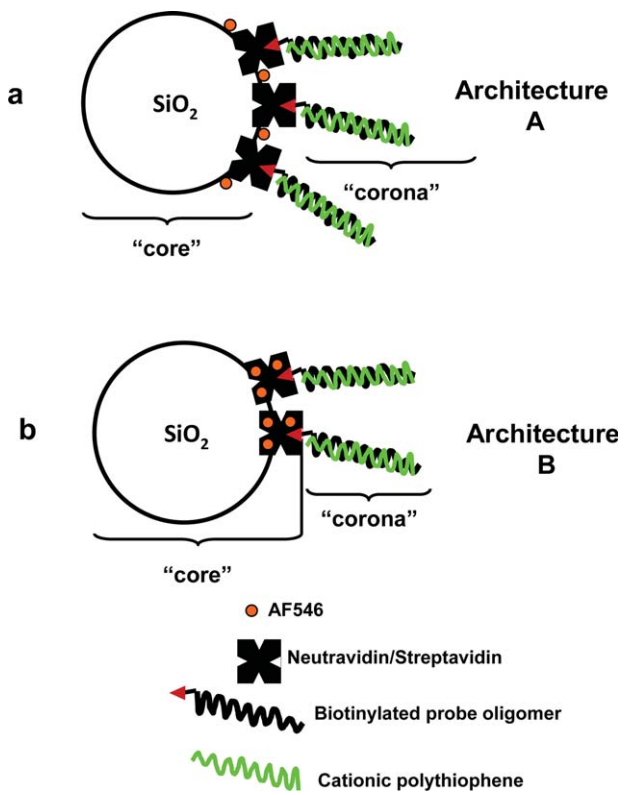

Fig. 1 The principles of the biosensing mechanism, where the surface of the nanoparticle is modified with AF546 in architecture A (a) and the AF546 is localized on the streptavidin anchor near the oligomer/polythiophene in architecture B (b).

FRET acceptor is anchored close to the nanoparticle surface through direct surface modification or through the attachment of an AF546-modified streptavidin molecule and each nanoparticle can be thought of as the core of the aggregate micelle structure depicted in Scheme 3. Post-modification of the nanoparticle surface with ss-oligomer probe and polymer then makes up the corona of the micelle, analogous to that illustrated in Scheme 3. These nanoparticle-fixed architectures are of interest because they allow us to elucidate how changing the number and proximity of FRET acceptors close to the FRET donor will influence the FRET efficiency and thus the emission intensity of the FRET acceptor following the introduction of unlabelled target ss-oligomer sequences that would allow for the detection of *Bacillus anthracis*.

Results and discussion

The silica nanoparticle scaffold employed in this investigation was prepared *via* the Stöber method and was 188 ± 30 nm in diameter as measured by TEM and 196 ± 36 nm in diameter measured by dynamic light scattering (Nanosight, UK). For the duration of the report, the nanoparticles are referred to as being ~200 nm. An amine group was introduced to the nanoparticle surface by adding 3-aminopropyltriethoxysilane directly to the crude reaction mixture. The resulting amine-modified nanoparticles were purified *via* repeated centrifugation cycles in ethanol to remove all unreacted APTES and ammonium hydroxide. The nanoparticles were then transferred to DMF and either co-reacted with both succinic anhydride and 3 different concentrations of AF546-*N*-hydroxysuccinimide (AF546-NHS, Invitrogen) (Architecture A) or modified with succinic anhydride to yield carboxylic acid-modified nanoparticles (Architecture B). Nanoparticle A was mixed with NeutrAvidin (Invitrogen) in the presence of 1-ethyl-3-(3-dimethylaminopropyl)carbodiimide hydrochloride (EDC) to co-modify the surface with both NeutrAvidin and AF546. Nanoparticle B utilized EDC to couple streptravidin-AF546 (Invitrogen) to the carboxylic acid groups (Scheme 4). Both streptavidin and NeutrAvidin are tetrameric proteins well known to interact strongly with biotinylated substrates and were subsequently used to anchor biotinylated probe ss-oligonucleotides (5′-biotin-C6 spacer-ACAAA TACCTGTAATTAGCGTTGCC-3′) to the surface of the nanoparticle to generate A_{probe} and B_{probe}, respectively. The general approaches to prepare these nanoparticles are highlighted in Scheme 4 and the detailed synthetic protocols are provided in the ESI†.

It has previously been reported that the ideal ratio of conjugated polymer to ss-oligomer is 1 : 1 with respect to charge.[7] That is, for each positive charge on the polymer backbone there should be an off-setting negative charge on the probe oligomer, resulting in an overall neutral charge in the duplex structure. To accurately elucidate the concentration of probe oligomer on each A_{probe} and B_{probe} nanoparticle prior to adding the conjugated polymer to generate the duplex structure, an aliquot of each nanoparticle was hybridized with a Cy5-modified complementary oligomer (3′-TGTTTATGGACATTAATCGCAACGG-Cy5-5′) and the concentration of bound target was quantified using UV-visible spectroscopy. The hybridization was carried out at room temperature in a buffer comprised of 30% formamide, 30% 15×

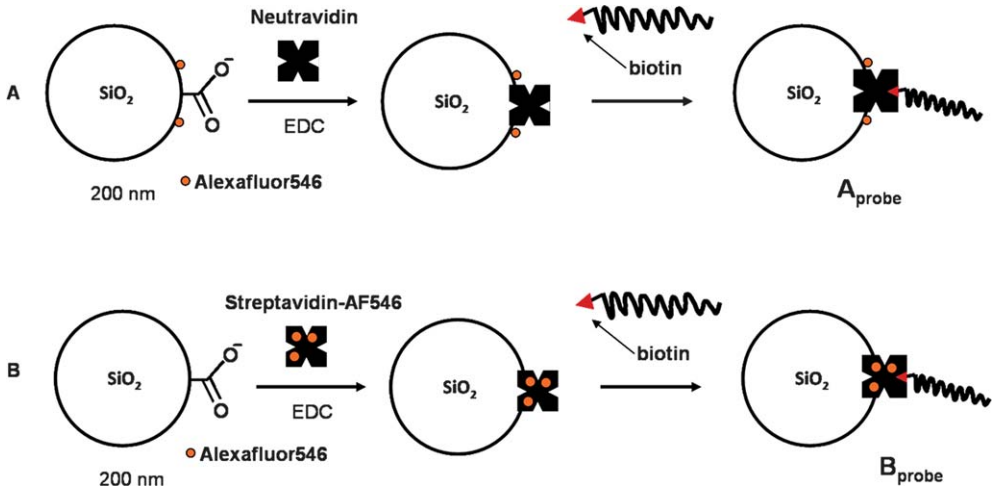

Scheme 4 A schematic representation of the reaction scheme employed to modify the surface of the nanoparticles with the FRET donor/acceptor biosensor. In (a) the ratio of the acceptor (AF546) to the donor (oligomer/polythiophene) can be tuned between 0.4 and 4.8 and in (b) the acceptor : donor ratio is 3.

SSPE buffer, 0.75% of a 4% polyvinylpyrrolidone solution and 39.25% MQ water with excess Cy5-modified target oligomer over two hours and the resulting hybridized nanoparticles were purified through repeated centrifugation cycles (four) in 1× PBS buffer with 1 M NaCl to remove any unhybridized target Cy5-modified oligomer. A UV-vis spectrum of the hybridized nanoparticles was then acquired and the concentration of Cy5-modified oligomer was quantified through the use of a calibration curve (details provided in the ESI†). This analysis also allows us to calculate the concentration of AF546 with respect to the concentration of oligomer, with the assumption that all of the ss-probe oligomer can form a duplex and hybridize with the complementary ss-target oligomer. That is, the FRET acceptor/donor ratio on A_{probe} and B_{probe} can be determined through comparison of the UV-vis absorption spectra and comparison of the relative absorption coefficients (*i.e.* $\varepsilon_{Cy5} = 250\,000$ and $\varepsilon_{AF546} = 104\,000$). A summary of these data is presented in Table 1 and in the ESI†. This characterization also allows the determination of the concentration of polythiophene that has to be added to produce charge neutral duplex structures on the nanoparticle surfaces. With the appropriate concentration of the conjugated polymer added to each nanoparticle scaffold generating the duplex (A_{duplex} and B_{duplex}), the response in the emission intensity at 572 nm (from the AF546 FRET acceptor, Scheme 2 and Fig. 1) is studied as the unlabelled target oligomer is added to produce $A_{triplex}$ and $B_{triplex}$, respectively. This preliminary experiment was used to determine the nanoparticle architecture best suited for label free oligomer detection and how the donor/acceptor ratio and spatial separation of the FRET pair affect the biosensing.

Table 1 Summary of the different AF546 : probe oligomer ratios for the various different nanoparticle architectures

Nanoparticle architecture	Ratio of AF546 : probe oligomer (FRET acceptor : donor)
A_{probe}	4.8
A_{probe}	1.5
A_{probe}	0.4
B_{probe}	3

To assess the ability of each nanoparticle to detect unlabelled ss-target oligomer, an emission spectrum of each derivative of A_{duplex} was first recorded upon excitation at 420 nm (absorption maximum of the polythiophene). These spectra are presented in Fig. 2 (black spectra in Fig. 2a–c). The spectra have emission peaks at 572 nm (direct excitation of AF546) and a weak, broad emission centered at ~530 (range between 500 and 600 nm) from the polythiophene. In general, following the addition of excess complementary unlabelled target ss-oligomer (3′-TGTTTATG-GACATTAATCGCAACGG-5′, final concentration of target oligomer is 10 nM, concentration of duplex is ~2 nM) there is an increase in emission intensity at 572 nm (due to FRET between the polythiophene donor and the AF546 acceptor) as well as an increase in emission intensity at 530 nm (due to the polythiophene itself). The emission intensity increase is quantified by comparing the relative emission intensity at 530 nm and 572 nm prior to and following the addition of target ss-oligomer. As demonstrated in Fig. 2 and shown in Table 2, the luminescent responses of the A_{duplex} derivatives at 572 nm are quite different as the acceptor/donor (AF546/duplex) ratio changes. Examination of the emission spectra in Fig. 2 suggests that after the addition of target oligomer, only the A_{probe} with ~1.5 and 4.8 AF546 (acceptor) molecules per duplex (donor) provides emission intensity increases that can be ascribed to effective FRET interactions between the AF546 and the polythiophene. In addition, only these nanoparticles provide emission intensity increases sufficient for label-free detection of complementary oligomer, particularly in the presence of competing noncomplementary ss-oligomers. The average emission intensity increase at 572 nm, which is ascribed to FRET between the polymer in the triplex ("on") state and the AF546, for each nanoparticle is ~1.5, 2.8 and 1.2 for acceptor : donor ratios of 4.8, 1.5 and 0.4, respectively. As described earlier, Leclerc *et al.* postulate that the sensitivity of this FRET-based biosensing is improved through the AF546 fluorophores aggregating at the interior of micelle-like duplex structures (Scheme 3), where the FRET acceptor was

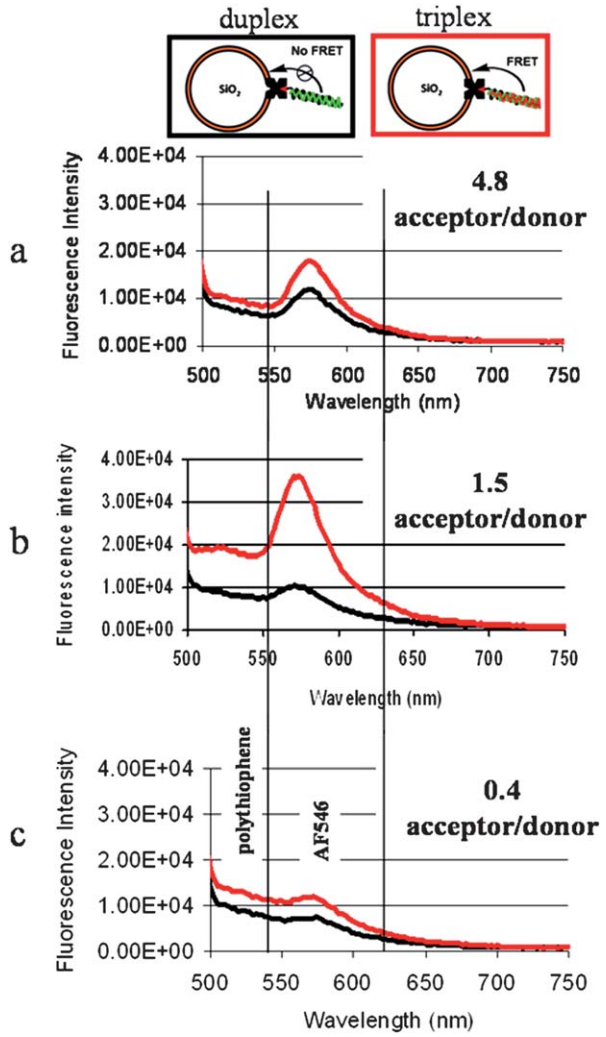

Fig. 2 The spectral responses for the A_{duplex} when the FRET acceptor (AF546)/donor (polythiophene) ratios are 4.8 (a), 1.5 (b) and 0.4 (c). For each series of spectra the black spectrum is the signal from A_{duplex} whereas the red spectrum is from $A_{triplex}$. Note that the emission intensity increase at ~530 nm is due to the polythiophene emission alone.

always close to the FRET donor, particularly when very few oligomer targets are present to activate the polymer fluorescence.[7] As such, it was expected that increasing the relative number of AF546 FRET acceptors on the nanoparticle surface with respect to the number of donors (polythiophene in the triplex state) would increase the FRET efficiency because the donors would always be close to many acceptors. However, this biosensor is most effective when the acceptor : donor ratio is ~1.5 : 1 (Fig. 2), where the relative fluorescence intensity of the AF546 acceptors increases by ~2.8-fold.

The effectiveness of this label free DNA biosensing scheme is dictated by the efficiency of FRET between the fluorescent state of the conjugated polymer in the triplex form and the AF546 fluorophore appended to the nanoparticle surface.[7] If efficient FRET is occurring between the polythiophene and AF546 moiety, there should be little to no emission at 530 nm from the polythiophene itself. However, as evidenced in Fig. 2 and highlighted in Table 2 there is generally an onset of both polymer emission (emission peak centered at ~530 nm) as well as an increase in emission intensity at 572 nm from the AF546 acceptor. Note that the fluorimeter settings used to probe the spectral responses following the addition of target oligomer for $A_{duplex(0.4)}$, $A_{duplex(1.5)}$ and $A_{duplex(4.8)}$ are not identical, so the absolute intensity increases are not important, but rather the relative intensity increases at each region in the spectra are. That is, to best elucidate what is occurring within each biosensing scenario ($A_{duplex(0.4)}$, $A_{duplex(1.5)}$ and $A_{duplex(4.8)}$) we compare the relative emission intensity increase for both the polymer (donor) emission at 530 nm and the AF546 (acceptor) emission at 572 nm. For $A_{duplex(0.4)}$, following the addition of the target oligomer there is an increase in the relative emission intensity at 530 nm from the polymer but essentially no change in the relative emission intensity at 572 nm for AF546 suggesting that the polymer emission turns on but does not effectively undergo FRET with AF546 (Fig. 2c). In contrast, for $A_{duplex(1.5)}$ the relative emission intensities at 530 nm and 572 nm both increase significantly. This suggests that both the polymer itself is emitting (530 nm) and FRET is occurring between some of the excited polymer (donor) and the AF546 molecules (acceptor), resulting in the relative emission intensity increase at 572 nm. Finally, for $A_{duplex(4.8)}$ the relative increase in emission intensity from the polymer itself at 530 nm is small in comparison to the relative increase in intensity at 572 nm, suggesting again that FRET is occurring. However, because there are significantly more acceptors in $A_{duplex(4.8)}$, it was expected that the relative increase in emission intensity at 572 nm for $A_{duplex(4.8)}$ would be greater than that for $A_{duplex(1.5)}$. To explain why the relative emission intensity increase may be lower than expected it is instructive to determine the spatial separation of the molecules on the nanoparticle surface. Note, it is important to highlight that the number of probe oligomers on each family of nanoparticles is essentially the same for $A_{probe(0.4,\ 1.5\ and\ 4.8)}$ and only the number of AF546 acceptors is increasing.

When the acceptor/donor ratio is low ($A_{probe(0.4)}$) calculations suggest that the separation between all of the molecules (acceptors and donors) on the nanoparticle surface is ~13 nm, which exceeds the maximum 10 nm generally required for effective FRET. This is consistent with what is observed in $A_{triplex(0.4)}$ upon introduction of the complementary target oligomer where there is an increase in emission intensity at 530 nm from the

Table 2 Summary of the spectral responses and molecular separations for the various different nanoparticle architectures

Nanoparticle architecture	Relative intensity increase at 530 nm	Relative intensity increase at 572 nm	Average separation between molecules on nanoparticle surface
$A_{duplex(4.8)}$	1.2	1.5	7 nm
$A_{duplex(1.5)}$	2.1	2.8	10 nm
$A_{duplex(0.4)}$	1.5	1.1	13 nm
B_{duplex}	1.7	1.9	4 nm

polythiophene itself and little if any intensity increase at 572 nm due to FRET (Fig. 2c). This also illustrates that in the absence of FRET, the intensity increase from the polymer alone at this concentration is insufficient to definitively determine if the ss-target oligomer is present. Conversely, as highlighted in Fig. 2b, $A_{duplex(1.5)}$ provides a high relative increase of 2.8 at 572 nm due to FRET but there is also a significant relative increase in emission intensity due to the polymer alone at 530 nm (Fig. 2b and Table 2). Here the average distance between the molecules on the nanoparticle surface is ~10 nm, approaching the maximum distance allowing for effective FRET. As such, the nanoparticles produce both FRET-based emission at 572 nm and polymer emission at 530 nm. Interestingly, for $A_{duplex(4.8)}$, assuming an equal distribution of the molecules over the entire nanoparticle surface, the separation between the molecules is ~7 nm, so the FRET donors and acceptors should be well within the distance for effective FRET. $A_{duplex(4.8)}$ has a relative polymer-based response that is low (suggesting effective FRET is occurring), but the actual relative emission intensity increase at 572 nm is also lower than expected. It is likely that at high acceptor : donor ratios ($A_{duplex(4.8)}$) there is fluorophore aggregation on the nanoparticle surface and this aggregation results in self-quenching of the AF546 molecules, producing a less intense emission. A report by Bringley and coworkers suggests that the quantum efficiency of similar cyanine fluorophores decreases significantly when the spatial separation of them within a silica nanoparticle matrix is less than 10 nm.[13] Imhof and coworkers also report that as the separation of fluorescein molecules reaches less than 10 nm, significant quenching of the fluorophore emission occurs.[14] In both investigations the authors propose that this decrease in quantum yield/emission intensity is the result of fluorophore aggregation on (and within) the nanoparticle.[13,14] Such data suggest that for ($A_{duplex(4.8)}$) the polymer (donor) and the acceptors (AF546) are close enough to participate in effective FRET, but when the AF546 molecules are in their excited states, the energy is lost due to self-quenching with other AF546 molecules (average separation is ~7 nm). Such aggregation-induced self-quenching accounts for the relative emission intensity increase at 572 nm not being as large as expected. Interestingly, the spatial separation between the AF546 molecules in $A_{duplex(1.5)}$ correlates well with data reported by Imhof *et al.*,[14] where separations of 10 nm or greater do not cause significant self-quenching, verifying that only some of the molecules will be close enough to each other to participate in FRET interactions. It has been reported that loading "Alexa" dye molecules (Invitrogen) onto biological molecules does not generally lead to significant quantum yield decreases resulting from self-quenching.[15] As such, we wanted to explore a nanoparticle architecture that could potentially better arrange the acceptors and donors in close proximity and decrease luminescence quenching inherent to architecture A to elucidate if the optical properties (*i.e.* FRET efficiency) and sensitivity of the nanoparticle-based biosensor could be improved.

In order to fix the FRET pair in close proximity, an AF546-modified streptavidin is first immobilized on the nanoparticle surface, which will in turn bind the probe ss-oligomer (B_{probe}), keeping the polythiophene close to the FRET acceptor (separation less than 4 nm) when B_{duplex} is generated (Fig. 1b and Scheme 4). Following the synthesis of B_{probe}, the number of probe oligomers on B_{probe} was also characterized through hybridization with a Cy5-labelled complementary oligomer in a process analogous to that described above for A_{probe}. From these data, and from the AF546 loading supplied with the modified streptavidin (3 AF546/mole of streptavidin), it was verified that the acceptor : donor (AF546 : probe oligomer) ratio was 3. Again, following the addition of unlabelled target oligomer (10 nM target oligomer) there is a significant increase in the luminescence intensity at 572 nm, suggesting that FRET occurs between the polythiophene in the triplex state and the AF546 acceptor molecules (Fig. 3). However, there is also an increase in the emission intensity at ~530 nm which is due to the polythiophene triplex alone. This suggests that FRET efficiency between the polythiophene and the AF546 may not be the limiting factor in this biosensor, because even when the FRET pairs are localized on the same biomolecule and separated by ~4 nm not all of the donor energy is transferred to the AF546 acceptor. There is however clear signal differentiation between the biosensor in its duplex state and the triplex state, suggesting that B_{duplex} is also an effective means of detecting oligomers in a label free manner (Fig. 3). Though the emission intensity does not increase as much as anticipated, it appears that immobilizing the AF546 onto the streptavidin moiety does improve the resulting emission intensity of the biosensor in comparison to $A_{probe(4.8)}$. As such, the limits of detection for unlabelled ss-target oligomers for both $A_{probe(1.5)}$ and B_{probe} were elucidated in a competition assay with a noncomplementary oligomer.

The limits of detection (LOD) for the two most effective nanoparticle biosensors were determined by using a constant concentration of A_{probe} or B_{probe} (concentration of probe oligomer ~2 nM) mixed with increasingly lower concentrations of unlabelled target ss-oligomer (sequence 3′-CTATCT GATTGTTGAAGAAGGATT-5′ or 3′-TTGATTATTGT TATCCTGTTATGCC-5′). These data are presented for both $A_{probe(1.5)}$ and B_{probe} in Fig. 4. A critical aspect to any DNA biosensor is the ability to distinguish between a complementary target and potential competing interactions such as a noncomplementary oligomer. As can be seen in Fig. 4, there is some response from presence of excess noncomplementary oligomer, but the biosensor is effective down to modest concentrations of

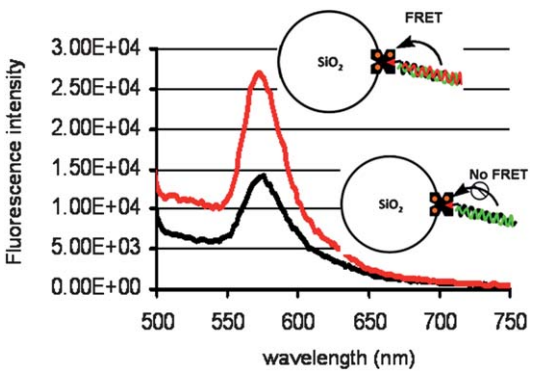

Fig. 3 The spectral responses for the B_{duplex} when the FRET acceptor (AF546)/donor (polythiophene) ratio is 3, as dictated by the number of AF546 fluorophores anchored to each streptavidin molecule. For each series of spectra the black spectrum is the signal from B_{duplex} whereas the red spectrum is from $B_{triplex}$. Note that the emission intensity increase at ~530 nm is due to the polythiophene emission alone.

~2 nM and 3 nM for $A_{duplex(1.5)}$ and B_{duplex}, respectively (calculating 3σ on the response from the noncomplementary oligomer). This is reasonable sensitivity, and considering it is label free represents a unique and effective means of detecting DNA from selected targets. It should also be highlighted that in most cases *Bacillus anthracis* is used in a biological attack, it is delivered in large, easily visible quantities, so a label-free detection assay, even with a nM limit of detection, is valuable.

For biowarfare agent detection there is an increasing need for the development of field deployable devices. As such, devices that utilize biosensors immobilized on solid substrates within microfluidic devices are of particular interest. Recent attempts to incorporate the micelle-based biosensor described in Scheme 3 onto a support that can be incorporated into a microfluidic device (a 10–20 μm bead support) have resulted in poor surface immobilization, irreproducible intensity increases in the presence of target oligonucleotides and poor differentiation between perfectly complementary target oligomers and noncomplementary control oligomers. This is due in large part to the instability of the micelles following interaction with the bead surface, particularly during washing procedures, which results in the loss of the core–shell architecture responsible for the sensing mechanism (Scheme 3). In contrast, following immobilization of the nanoparticle-based biosensors described in this report onto the bead surface, the nanoparticle sensors remain functional due to their covalent assembly.

The synthesis of this nanoparticle-on-magnetic bead (n-MB) conjugate is described in detail in the ESI†. In general, the carboxylic acid-modified 20 μm magnetic beads (Kisker, cat# PMC-18.0) were decorated with 200 nm amine-modified silica nanoparticles in MES buffer and subsequently modified with AF546-NHS and succinic anhydride to produce a surface co-modified with both AF546 and a carboxylic acid (Fig. 5). Note that the conditions to produce the AF546/COOH decorated n-MBs were identical to that to produce $A_{probe(1.5)}$, so the acceptor : donor ratio is close to 1.5. Finally the n-MBs were modified with NeutrAvidin and the probe oligomer (5′-biotin-C6 spacer-ACAAATACCTGTAATTAGCGTTGCC-3′) to generate $n\text{-}MB_{probe}$ (Fig. 5). As highlighted in Fig. 5, the nanoparticle coverage on each n-MB is excellent. In contrast to the investigation of the micelles immobilized on the microbead surface, the

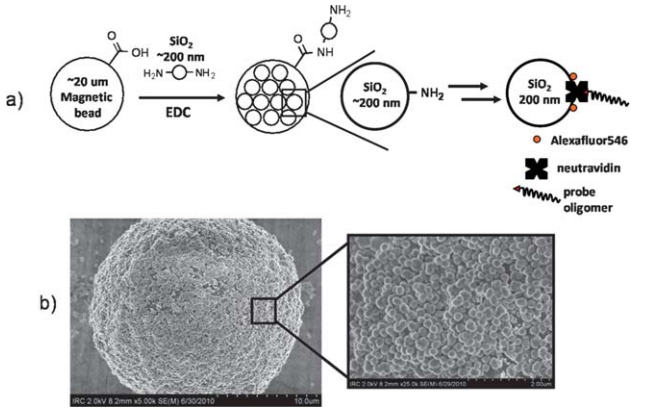

Fig. 5 A schematic demonstrating the construction of $n\text{-}MB_{probe}$ where 200 nm silica nanoparticles are covalently attached to 20 μm magnetic beads and subsequently modified with probe ss-oligomers for solid support based label-free detection of target DNA (a) and an SEM image of the $n\text{-}MB_{probe}$ used in the biosensing assay (b).

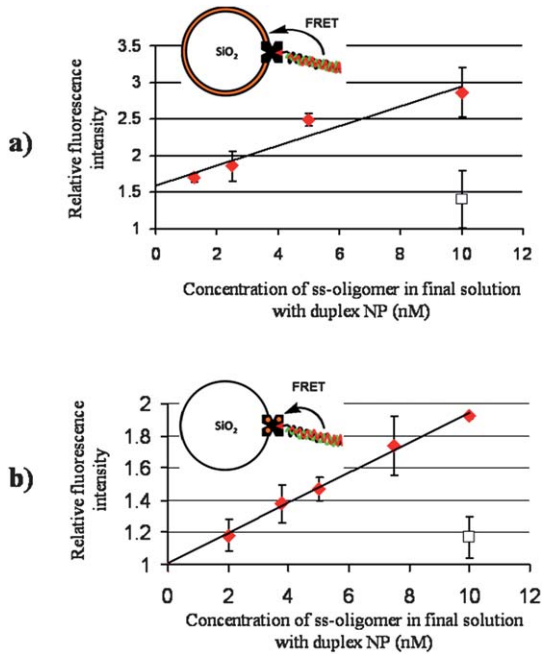

Fig. 4 The limit of detection curves for $A_{duplex(1.5)}$ (a) and B_{duplex} (b). In both curves the red squares represent the relative luminescence intensity increase following the addition of unlabelled complementary target ss-oligomers and the white squares represent the relative luminescence intensity increase following the addition of noncomplementary ss-oligomers. Note that these sensing assays were carried out by first adding the noncomplementary strand, and subsequently adding the complementary target oligomer.

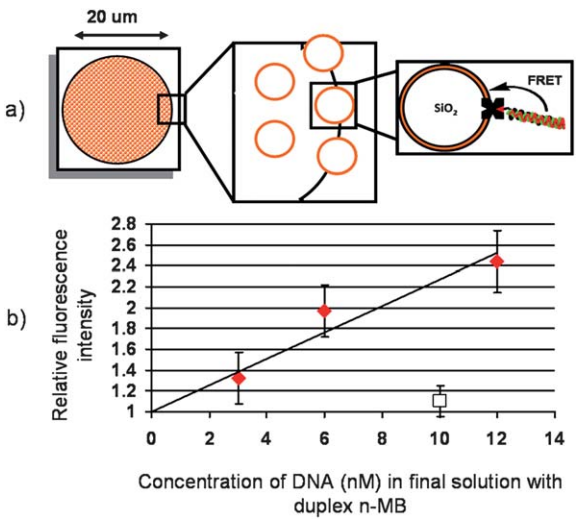

Fig. 6 A schematic representation of the n-MB architecture (a) and the limit of detection curve for $n\text{-}MB_{duplex}$ (b). In the chart the red squares represent the relative luminescence intensity increase following the addition of unlabelled complementary target ss-oligomers and the white square represents the relative luminescence intensity increase following the addition of noncomplementary ss-oligomers. Note that this sensing assay was carried out by first adding the noncomplementary strand, and subsequently adding the complementary target oligomer.

n-MB_{probe} could not only detect the presence of unlabelled target oligomer, but the limit of detection on the solid support remains close to that of the free nanoparticle in solution (~5 nM, Fig. 6). Note that the standard deviation of each point is slightly higher when the nanoparticle-based biosensor is immobilized on the beads. We attribute this to a combination of scattering of light from the large beads and the fact that the beads are so large that they slowly precipitate from solution, which can cause slight variation in intensities over the duration of the spectrum acquisition. Interestingly, when the nanoparticles are immobilized on a magnetic support, magnetic preconcentration measures can be carried out in order to improve the sensitivity of detection. There are big advantages to using these nanoparticle-on-bead scaffolds, where it is possible to magnetically confine the sensors from 1–2 mL of water and redisperse them in 100 μL of water. Though the limit of detection for the actual experiment would remain ~5 nM in the concentrated state, it is possible to detect the target oligomers that were originally present in solution at 0.3–0.4 nM.

Conclusions

Within this report we describe the preparation of the ss-oligomer-modified nanoparticles decorated with Alexa Fluor 546 FRET acceptors and the subsequent preparation of a polythiophene biosensor "duplex" moiety capable of providing a fluorescence response in the presence of unlabelled complementary ss-oligomers. It has been demonstrated that tuning the proximity and ratio of the FRET acceptor/donor pairs is important in the sensing mechanism. If too few acceptors are present the biosensing relies solely on the polymer biosensor where positive responses at low (10–15 nM) concentrations are difficult to distinguish. Conversely, too many acceptors lead to more effective FRET between the polymer donors and AF546 acceptors, but self-quenching among the acceptors leads to a decrease in the relative fluorescence intensity of the AF546 acceptor, resulting in poor biosensing. The optimum sensor in this study provides a tradeoff between the spatial separation of the FRET pairs and the donor : acceptor ratio. Though the FRET efficiency is far from 100%, these nanoparticle-based biosensors can readily discriminate between perfectly complementary target ss-oligomers and noncomplementary ss-oligonucleotides in a competition assay with nanomolar limits of detection employing a standard fluorimeter with no specialized equipment or experimental setups. This nanoparticle scaffold can provide a number of significant advantages where sample isolation/manipulation is concerned. For example, the nanoparticles can be immobilized on a magnetic bead (Fig. 5) allowing for magnetic preconcentration or manipulation within microfluidic devices. Such a label-free detection scheme provides a valuable new tool that can allow for the sensitive detection of DNA without the use of PCR, and could be incorporated into a deployable device for the on-site detection of biological warfare agents such as *Bacillus anthracis*.

Acknowledgements

This work was supported by Defence Research and Development Canada Centre for Security Science Chemical, Biological, Radiological/Nuclear, and Explosives Research and Technology Initiative (CRTI-03-0005RD and CRTI-06-0187TD). LP thanks the National Research Council for funding as a summer student. The authors also wish to thank Dr Yun Liu (Materials Characterization Core Facility at the University of Ottawa) for acquiring the TEM images, Mr Gordon Chan (Institute for Research in Construction, National Research Council) for acquiring the SEM images and Dr Chantal Paquet and Dr Even Lemieux for discussions and suggestions.

References

1 H. Li and G. C. Bazan, *Adv. Mater.*, 2009, **21**, 964–967.
2 B. S. Gaylord, A. J. Heeger and G. C. Bazan, *Proc. Natl. Acad. Sci. U. S. A.*, 2002, **99**, 10954–10957.
3 C. Chi, A. Chworos, J. Zhang, A. Mikhailovsky and G. C. Bazan, *Adv. Funct. Mater.*, 2008, **18**, 3606–3612.
4 A. Duarte, A. Chworos, S. F. Flagan, G. Hanrahan and G. Bazan, *J. Am. Chem. Soc.*, 2010, **132**, 12562–12564.
5 U. H. F. Bunz and V. M. Rotello, *Angew. Chem., Int. Ed.*, 2010, **49**, 5037–3279.
6 R. L. Phillips, O. R. Miranda, C. C. You, V. M. Rotello and U. H. F. Bunz, *Angew. Chem., Int. Ed.*, 2008, **47**, 2590–2594.
7 H.-A. Ho, A. Najari and M. Leclerc, *Acc. Chem. Res.*, 2008, **41**, 168–178.
8 K. Doré, R. Neagu-Plesu, M. Leclerc, D. Boudreau and A. M. Ritcey, *Langmuir*, 2007, **23**, 258–264.
9 S. Dubus, J. F. Gravel, B. Le Drogoff, P. Nobert, T. Veres and D. Boudreau, *Anal. Chem.*, 2006, **78**, 4457–4464.
10 X. Yanga, X. Zhaoa, X. Zuoa, K. Wang, J. Wen and H. Zhang, *Talanta*, 2009, **77**, 1027–1031.
11 Y. Wang and B. Liu, *Chem. Commun.*, 2007, 3553–3555.
12 D. Brouard, M. L. Viger, A. G. Bracamonte and D. Boudreau, *ACS Nano*, 2011, **5**(3), 1888–1896.
13 J. F. Bringley, T. L. Penner, R. Z. Wang, J. F. Harder, W. J. Harrison and L. Buonemani, *J. Colloid Interface Sci.*, 2008, **320**, 132–139.
14 A. Imhof, M. Megens, J. J. Engelberts, D. T. N. de Lang, R. Sprik and W. L. Vos, *J. Phys. Chem. B*, 1999, **103**, 1408–1415.
15 N. Panchuk-Voloshina, R. P. Haugland, J. Bishop-Stewart, M. K. Bhalgat, P. J. Millard, F. Mao, W. Y. Leung and R. P. Haugland, *J. Histochem. Cytochem.*, 1999, **47**, 1179–1188.

